PHYSICAL REVIEW E **78**, 046709 (2008)

Interaction potential for atomic simulations of conventional high explosives

Andrew J. Heim,[1,2] Niels Grønbech-Jensen,[1] Edward M. Kober,[2] Jerome J. Erpenbeck,[2] and Timothy C. Germann[2]
[1]*Department of Applied Science, University of California, Davis, California 95616, USA*
[2]*Theoretical Division, Los Alamos National Laboratory, Los Alamos, New Mexico 87545, USA*
(Received 24 June 2008; published 28 October 2008)

In an effort to develop a chemically reactive interaction potential suitable for application to the study of conventional, organic explosives, we have modified the diatomic *AB* potential of Brenner *et al.* [Phys. Rev. Lett. **70**, 2174 (1993); **76**, 2202(E) (1996)] such that it exhibits improved detonation characteristics. In particular, equilibrium molecular dynamics (MD) calculations of the modified potential demonstrate that the detonation products have an essentially diatomic, rather than polymeric, composition and that the detonation Hugoniot has the classic, concave-upward form. Nonequilibrium MD calculations reveal the separation of scales between chemical and hydrodynamic effects essential to the Zel'dovitch, von Neumann, and Döring theory.

DOI: 10.1103/PhysRevE.78.046709 PACS number(s): 47.40.Rs, 47.50.Cd, 82.40.Fp, 47.11.Mn

I. INTRODUCTION

For over 15 years, the reactive empirical bond-order (REBO) potential of Brenner *et al.* [1], or variations thereof, have been used for molecular dynamics (MD) simulations of detonation. It has been shown to follow the Chapman-Jouguet (CJ) theory and even that of Zel'dovich, von Neumann, and Döring (ZND) [2]. Being an MD model, it has at least two major shortcomings, namely its spatial and temporal scales. As computers become more powerful and codes and algorithms become more advanced, some of the restrictions that limit these scales can be loosened, allowing for more realistic behavior to be modeled.

While providing an atomic scale model of a reactive material, the empirical and classical model of Brenner *et al.* falls short of including all aspects of an accurate representation. Additionally, the spatial and temporal scales of real explosions make MD simulations a large computational task; but MD is still a useful tool for probing the characteristics of the detonation phenomenon, and the REBO potential is one of the best at balancing realism in the potential with accessibility to the large scale; yet there is room for improvement.

MD has certain conceptual advantages over hydrodynamics approaches that are parametrized to match the behavior of real high explosives. Even though the latter models can mimic real experiments on the proper spatial and temporal scales, they make assumptions about the reaction rate and multiphase equation of state (EOS) to do so. Some of these assumptions are parameter fittings, which may not elucidate any new physical intuition about detonation of the high explosive (HE) in question. In comparison, MD simulations depend on the parametrization of an interaction potential, which is arguably easier to connect directly to physical considerations than is a multiphase and multispecies EOS.

REBO has been used by many groups to model a variety of parametrizations and experimental configurations. However, a major criticism of this potential is that it has a thin reaction zone ($\sim$100 Å) relative to typical real high explosives ($\sim$1 mm) [10]. In previous works [3,4] several unconventional characteristics of the default parametrization of Brenner *et al.* [1] (called ModelI as in Ref. [4]) are made evident.

(1) ModelI displays nearly instantaneous dissociation upon compression by an unsupported detonation. Its entire reaction zone is characterized by a dissociative state.

(2) Its reaction zone is thin.

(3) It readily allows for clustering.

(4) Its CJ state is highly compressed.

(5) It has clearly nonhyperbolic equilibrium Hugoniots ($\mathcal{H}$) in P-v space.

None of these characteristics are proven to be unrealistic. In fact for some primary high explosives, the plasmalike state seen in ModelI of CJ may be realistic [5]. Clustering, particularly of carbon, is a real phenomenon in the thermal decomposition of some HEs [6,7]. However, successful models of conventional explosives have either assumed or suggested that more molecular states [8,9] with hyperbolic $\mathcal{H}$'s in P-v space [10–12] are typical and that compressions at CJ conditions should be $\approx$25% (for example, pentaerythritol tetranitrate (PETN) [11]) rather than $\approx$43% as with ModelI [3]. Given that ModelI can model a dissociated state, it would be useful to show that a more molecular state can also be modeled. The task of this work is to make modifications to the ModelI potential in order to accomplish this goal. Although, for the last feature in the above list, it is difficult to predict what changes would adjust it, an attempt to address the former features is made by making adjustments based on physical reasoning (see Sec. II). In Sec. IV the effects that the changes to the model of Brenner *et al.* have on the thermodynamic properties are investigated by the methods outlined in Sec. III. Notable results of nonequilibrium MD simulations are studied in the following paper [13].

II. CHANGING REBO: PHYSICAL AND AESTHETIC REASONING

In this section we motivate changes to the ModelI potential to form a different potential (called ModelIV after the naming scheme of White *et al.* [4]), the total bonding energy of which takes the form

TABLE I. The components and parameters used in Eq. (1). Mass of A: 14.008 amu; Mass of B: 12.010 amu; $\epsilon=5.0\times 10^{-3}$ eV; $c=200$; $D_e^{\mathrm{AA}}=D_e^{\mathrm{BB}}=5.0$ eV; $D_e^{\mathrm{AB}}=1.0$ eV; $\mathcal{D}_e=D_e+c\epsilon$; $S=1.8$; $\beta=2.7$ Å^{-1}; $r_e=1.2$ Å; $G=5.0$; $m=2.25$ Å^{-1}; $n=0.5$; $\bar{B}_{ij}=\frac{1}{2}(B_{ij}+B_{ji})$; $\gamma_1=1.3r_e$; $\gamma_2=1.7r_e$; $r^*=2^{1/6}\times 2.988$ Å; $\alpha_2=2^{-1/6}r^*$; $\alpha_1=0.683\alpha_2$; $\alpha_3=(\frac{13}{7})^{1/6}r^*$; $\alpha_4=\frac{67}{48}\alpha_3$; $P_3=-2290.707\,325\,617\,024$ Å^{-3}; $P_4=3603.929\,410\,034\,915$ Å^{-4}; $P_5=-1513.930\,039\,501\,751$ Å^{-5}; $C_0=2.575\,275\,778\,983\,429$; $C_1=-4.316\,677\,142\,326\,428$ Å^{-1}; $C_2=1.376\,573\,417\,835\,169$ Å^{-2}; $C_3=-0.123\,400\,881\,288\,945\,69$ Å^{-3}.

$$V_R(r)=\frac{\mathcal{D}_e}{S-1}\exp[-\beta\sqrt{2S}(r-r_e)]$$

$$V_A(r)=\frac{S\mathcal{D}_e}{S-1}\exp\left[-\beta\sqrt{\frac{2}{S}}(r-r_e)\right]$$

$$B_{ij}=\{1+G\textstyle\sum_{k\neq i,j}f_c(r_{ik})\exp[m(r_{ij}-r_{ik})]\}^{-n}$$

$$y(r)=\frac{r-\gamma_1}{\gamma_2-\gamma_1}$$

$$f_c(r)=\begin{cases}1 & y(r)<0\\ [1-y(r)]^3[1+3y(r)+6y^2(r)] & 0\leqslant y(r)<1\\ 0 & 1\leqslant y(r)\end{cases}$$

$$V_{vdW}(r)=\begin{cases}\epsilon c & r<\alpha_1\\ \epsilon(c+\sum_{i=3}^{5}P_i(r-\alpha_1)^i) & \alpha_1\leqslant r<\alpha_2\\ \epsilon\left[\left(\frac{r^*}{r}\right)^{12}-2\left(\frac{r^*}{r}\right)^{6}\right] & \alpha_2\leqslant r<\alpha_3\\ \epsilon(C_0+C_1r+C_2r^2+C_3r^3) & \alpha_3\leqslant r<\alpha_4\\ 0 & \alpha_4\leqslant r\end{cases}$$

$$E_b=\sum_i^N\sum_{j>i}^N\{f_c(r_{ij})[(2-\bar{B}_{ij})V_R(r_{ij})-\bar{B}_{ij}V_A(r_{ij})]+V_{vdW}(r_{ij})\}. \tag{1}$$

The parameters for Eq. (1) can be found in Table I. Before mentioning the physical basis for the modifications made to ModelI, let us list the features that ModelI already takes into account. In tests using ModelI, the parametrization is set to a valence of one, which should prefer dimers because one atom's sharing of electrons with one other fills both atoms' valence shells. The bonding energy takes the form

$$E_b=\sum_i^N\sum_{j>i}^N\{f_c(r_{ij})[V_R(r_{ij})-\bar{B}_{ij}V_A(r_{ij})]+V_{vdW}(r_{ij})\}. \tag{2}$$

See Table I in the errata of Brenner *et al.* [1] for the functions and components of Eq. (2). In ModelI this bond-order behavior is implemented by reducing the strength of the attractive term of a Morse potential used to model such covalent bonding. This is accomplished with a bond-order coefficient ($\bar{B}_{ij}$) that varies from one to zero with increasing proximity and number of neighbors.

Rice *et al.* found that ModelI allowed for trimer formation and subsequently strengthened this bond-order effect by increasing the repulsive term as well in order to better model bond saturation so that a particle became less likely to bond to more than one other [14,15]. The contribution of Rice *et al.* is a simplified adjustment for what can be a complicated interaction. For instance, the $\bar{B}_{ij}$ coefficient does not take spin or degeneracy into account. However, this type of correction is similar to the "bond saturation" term that is used in the more sophisticated and calibrated reactive force field (ReaxFF) potential of van Duin *et al.* [16].

In combination with this bond-order functionality, the variation of bond well depths allows for reactive chemistry. If i and k are different types of atoms, their respective well depths with j will be different. If j is deeper with k than with i, k will require less kinetic energy to displace i than i would have had their rolls been reversed. That difference in energy will be converted into the kinetic energy of the system, an exothermic reaction. This is the type of reaction modeled by ModelI, $2AB\rightarrow A_2+B_2+2Q$, where $Q\equiv D_e^{AA/BB}-D_e^{AB}$ is the exothermicity of the reaction. The amount of energy needed to dissociate AB is D_e^{AB}. To dissociate AA or BB requires $D_e^{AA/BB}$. These numbers ignore the small contribution of the V_{vdW} term in Eq. (2).

In ModelI the van der Waals (vdW) interaction is represented by a Lennard-Jones (LJ) form. It is connected with a terminating third-order polynomial with negative curvature in the short range domain so that the overly repulsive twelfth-order term does not compete with the Morse potential, which handles the covalent bonding and Pauli exclusion repulsion. The LJ form is parametrized to allow for solid lattice formation at low temperature. It turns out that the third-order inner spline introduces an artifact in ModelI since it has a section of positive slope, which allows it to trap particles (see Fig. 1) because of the resulting attractive force. It is only first-derivative continuous at the spline point and is cropped at the cutoff point.

ModelI simulates well the repulsion between individual atoms separated by less than their equilibrium distance—which depends on the number and proximity of neighbors to the pair. It does not, however, represent the electrostatic repulsion between dimers that occurs as their charge clouds overlap on approaching each other while still being too far away to rearrange bonds, ~3 Å. As a result there is no significant interaction between molecules at the range and magnitude that gives rise to high pressure dense molecular HE product fluid mixtures [17]. There are some good models for this, for example, that of Ziegler, Biersack, and Littmark (ZBL) [18] and ReaxFF [16]. In an attempt to improve upon ModelI and its results, we design a model (ModelIV), which incorporates, along with the aforementioned contribution of Rice *et al.*, the following modifications.

The inner spline is replaced with a repulsive core, which smoothly connects the negative (the zero of the potential energy is the dissociated state) LJ curve to a constant plateau in the region in which the Morse potential dominates. This inner core has no sections of positive slope—that is, sections of attractive force—and therefore cannot trap atoms, and it crudely models electrostatic repulsion.

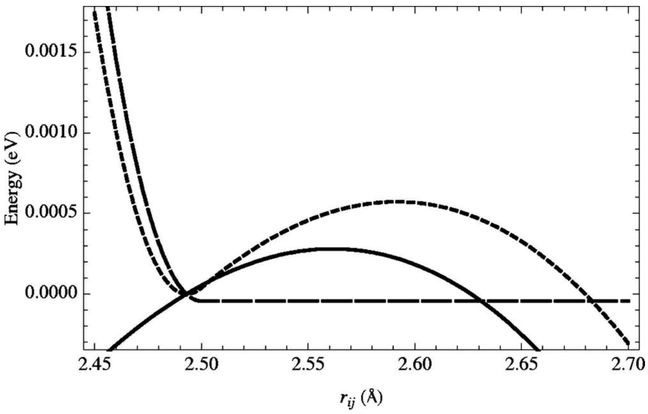

FIG. 1. Total bond energy in a 1D, three-particle, *A*-*B*-*A*, ModelI interaction in which the distance between the *B* and one of the *A*'s is fixed at the bond's equilibrium distance vs the distance between *B* and the remaining *A* (short dashed line). V_{vdW} for any two atoms (solid line). Total bonding energy less the V_{vdW} contributions (long dashed line). All curves are subtracted by their corresponding values at the position of the local minimum of the first curve for comparison purposes. This shows that the section of positive slope in the REBO V_{vdW} inner spline can trap particles. Without it, there is no trap.

The reason for connecting to a plateau is that it allows one to dictate the depth of the bonding potential. It also simplifies the definition of a covalent bond. Any two particles that are within the defined bond distance (see the f_c term in Table I) with a radial component of kinetic energy less than the height of the plateau are considered bonded. This definition also distinguishes bonded particles from particles that are merely confined by neighbors, and it can be determined at any instant. The height of the plateau, 1 eV, is chosen to be comparable to the thermal energy at the CJ state for ModelI [3], an addition that should decrease the reaction cross section, desensitizing the HE to initiation and, perhaps, adjusting reaction time and thus the width of the reaction zone. Perhaps a more physical function would continue to increase monotonically to a finite value at $r=0$ and have V_{vdW} be particle-type dependent.

All of the spline points in ModelIV have, at least, continuous second derivatives, with the exception of the outermost cutoff point. To terminate the V_{vdW} term in the long range, a Holian-Evans spline [19], which is second derivative continuous at its inner spline point but only first derivative continuous at its outer one, is used. A computational advantage for using the Holian-Evans spline is that the reach of the ModelIV potential is shorter (≈5.19 Å) than ModelI's (≈7.32 Å). Figure 2 shows a comparison of the two vdW potentials and Fig. 3 shows the corresponding forces. One can see that the ModelIV V_{vdW} term is still smooth in the force. As with the spline points in the V_{vdW} term, the cutoff function in the bond-order function and Morse potential is also replaced so that it is second-order continuous. Second derivative continuity helps energy conservation in the MD simulations (and allows longer time steps to be taken).

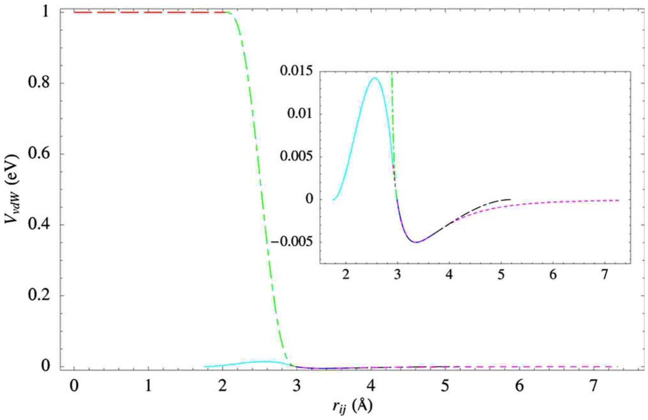

FIG. 2. (Color online) van der Waals (V_{vdW}) potential vs the interatomic distance (r_{ij}). Spline points are indicated by changes in color-dashing. ModelI V_{vdW} is made of a third-order polynomial (cyan-solid line) connected to a Lennard-Jones (LJ) form (mauve-short dashed line), which is cropped at a finite distance at which the slope and value of V_{vdW} are nearly zero. ModelIV V_{vdW} starts as a constant (red-long dashed line) and is connected with a fifth-order polynomial (green-long short dashed line) so that the spline points are second-derivative smooth, to a LJ form (blue-short short long dashed line) at zero, below which it coincides with the ModelI LJ form until the inflection point, at which it is connected to a curve (black-long long short dashed line) that is brought smoothly to zero within a finite distance, a Holian-Evans spline [19].

Another difference between ModelIV and ModelI is the depth of the metastable covalent wells. With the addition of the repulsive core, ModelIV fails to detonate with a well as deep as the default value for ModelI. The metastable well is raised by 1 eV, such that $D_e^{AB}=1.0$ eV, $D_e^{AA/BB}=5.0$ eV, and therefore, $Q=4.0$ eV. Comparing the potential energy surface for the linear, symmetric, metastable configuration for ModelI (see Fig. 4) to the one for ModelIV (see Fig. 5), we notice that the depression near $(1.2r_e, 1.2r_e)$ diminishes somewhat for ModelIV and that the barrier to be overcome for one particle to displace another via an end-on attack is significantly increased. All of these changes have notable effects on the EOS and detonation properties of the model HE. The final difference is that the masses of the particles are changed so that they are different from each other. The changes to ModelI to form ModelIV may be summarized as follows.

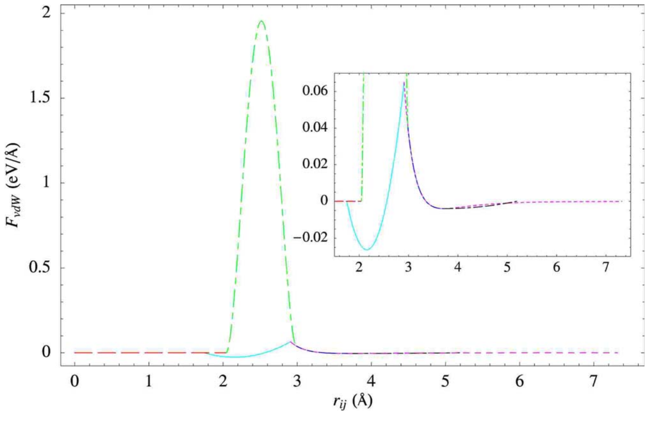

FIG. 3. (Color online) Forces that correspond to the potentials in Fig. 2.

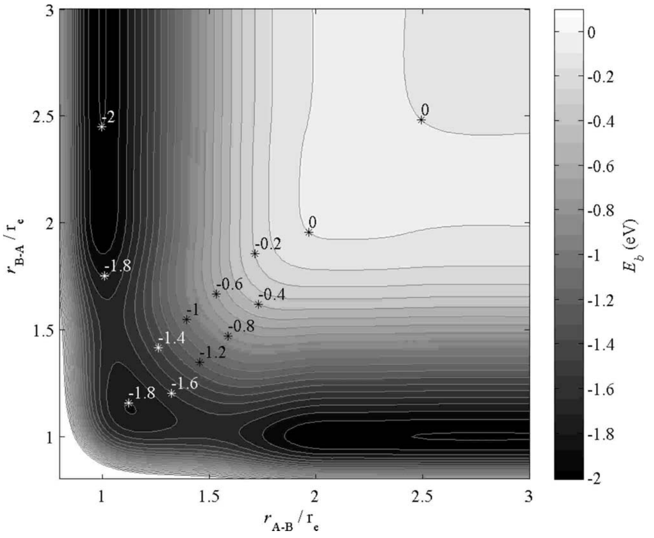

FIG. 4. Potential energy surface for the linear, symmetric, metastable configuration of ModelI atoms. The contours are spaced every 0.1 eV. $r_{A\text{-}B}$ is the distance between and A and B atom. $r_{B\text{-}A}$ is the the distance between the same A atom and a different B atom. r_e is the equilibrium distance for the metastable covalent interaction.

(1) A bond-order coefficient is applied to the repulsive term in the Morse part of the interaction potential.

(2) The inner spline of the V_{vdW} term is replaced with a repulsive core, which comprises a plateau connected to a LJ form with a monotonically decreasing fifth-order polynomial.

(3) The order of all of the splines is increased such that all but one spline point (the outermost cutoff) have smooth second derivatives.

(4) The masses of the atom types are changed so that they are no longer equal.

(5) The depth of the binding energy for the metastable bonds is made shallower.

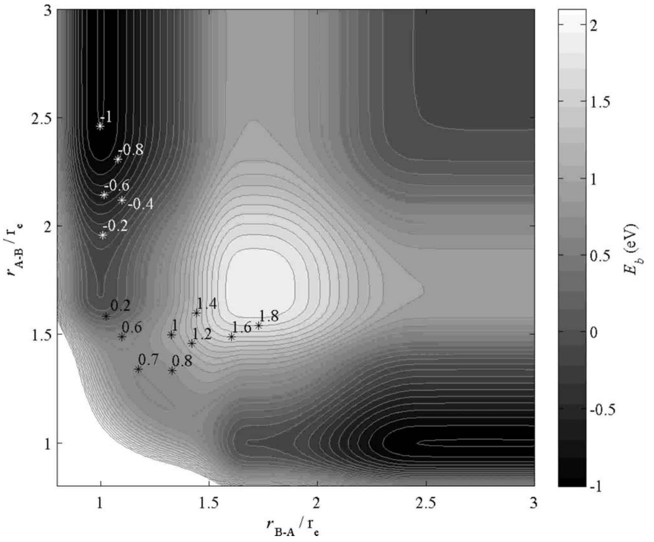

FIG. 5. Potential energy surface for the linear, symmetric, metastable configuration of ModelIV atoms. The contours are spaced every 0.1 eV.

III. METHODS

Investigating the two REBO potentials of which this paper is a study, ModelI and ModelIV, we use scaleable parallel short-range molecular dynamics code (SPaSM) 3.0 [20] to carry out the MD simulations, of which there are two main types, microcanonical ensembles (NVE) and nonequilibrium MD (NEMD). The NVE simulations are used for testing the thermochemical properties of a model and NEMD are used to investigate its detonation behavior. Both utilize the leapfrog Verlet method to advance the atoms' positions and momenta.

We conduct two subtypes of NVE simulations. The first is meant to find the equilibrium Hugoniots and is similar to those described by others [3,14,21]. The new model requires a shorter time step $\delta t \approx 0.16$ fs than does that of Brenner *et al.* [1], $\delta t \approx 0.25$ fs because of the relatively high curvature of the fifth-order spline in ModelIV's V_{vdW} term. Its zero-pressure configuration is also slightly different. The length of the sides of the rectangular unit lattice cell are $l_x = 6.191\,22$ Å and $l_z = 4.205\,38$ Å. The cell contains two dimers in a herringbone configuration. The angles that the dimers make with the horizontal are $\pm 27.7109°$. The atoms are placed 0.599 76 Å from the centers of their respective dimers, which are positioned at $(1/4l_z,\ 1/4l_x)$ and $(3/4l_z,\ 3/4l_x)$ from the lower left corner of the cell. These values are determined by isothermal-isobaric Monte Carlo simulations.

The second type of NVE simulation, the cookoff, is used to determine the reaction rate. The initial conditions are the same as with the first type of NVE except that the constituents are 100×100 cells^2 of AB not 25×25 of AA and BB. The time step is also drastically reduced so that good statistics can be found for measurements taken during rapid reactions. The time step varies among cookoff simulations, 6×10^{-4} fs $< \delta t < 0.02$ fs.

One of the purposes of creating a new potential is to expand the reaction zone by lowering the reaction cross section. This requires larger NEMD simulations to be performed. As Rice *et al.* have done [14] for computational efficiency, we try to reduce the amount of preshocked material modeled by tacking initial state material onto the end of the sample as the shock front approaches. To reduce surface effects, we introduce at the surface a one-cell-thick layer of two new particles, C and D, that have all of the properties of A and B, respectively, except that they start frozen and their velocities are not updated. When the shock front nears the frozen layer, the frozen layer is converted to A and B and is thermalized along with the new material. Another frozen layer is tacked onto the end. The size of a NEMD simulation is discretely dependent on time. The largest simulation contained over 3×10^6 atoms.

Another effect of decreasing the reaction cross section is that the incubation time, before which detonation occurs, extends. The sensitivity to impact is thus lessened. To overcome this, we initially overdrive the simulation with a piston that moves into the material at a velocity $u_{\text{pstn}} \approx 4.9$ km/s. After a detonation front has seemingly been established, it is smoothly backed off by following a sine-shaped deceleration over 200 time steps to a desired velocity. The time step is the same as with the first type of NVE simulation, $\delta t \approx 0.16$ fs.

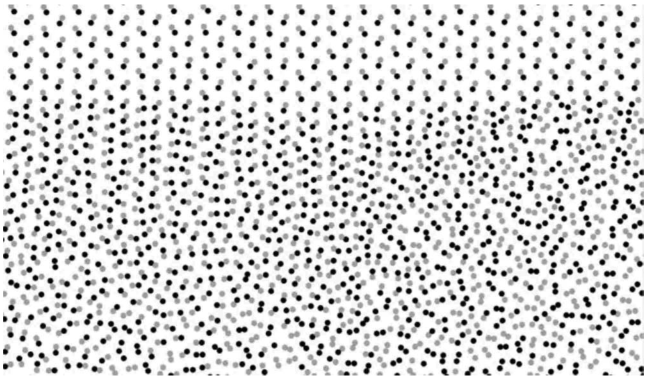

FIG. 6. Snapshot of a section of a shock front for an undersupported detonation using the ModelIV potential. Shock is propagating upward. Particles are shaded by atom type.

Most of the results of the NEMD simulations are reported in the following paper [13].

IV. COMPARISON OF THERMODYNAMIC PROPERTIES

We start the comparison of the properties of ModelI and ModelIV by analyzing how the ModelIV material behaves when compressed by the passage of an underdriven detonation front. From the snapshot of a NEMD simulation using ModelIV (see Fig. 6), one can see on the left half that many unreacted dimers are lining up horizontally. This is representative of uniaxial compression. Farther back it has melted, and farther back still reacted products are evident. On the right half, the dimers do not seem to line up before reacting. It is made evident in the following paper [13] that this is an effect of detonation instability and the propagation of transverse waves. When comparing this to a snapshot of detonation in ModelI (see Fig. 1 in the paper of Heim *et al.* [3]), one notices that, even at the right side of the sample, ModelIV seems to hold its molecular identity better than ModelI during compression by a detonation front that is not overdriven. It seemingly displays a greater resilience to dissociation. Both the right half of the ModelIV snapshot and the ModelI snapshot lack a significant induction zone.

To better compare the widths of the detonation fronts of the two models, profiles of the average z component of particle velocity from a critically supported detonation of ModelIV are plotted. Figure 7 indicates that the reaction zone is about 700 Å wide since that is the position at which the curves settle down to the constant u_{pj}. With the same method, the width of the reaction zone for ModelI was determined to be about 300 Å [3].

Although ModelIV's reaction zone is still small compared to that of real explosives, it can be widened. To widen the reaction zone farther, one can create a reaction that requires more steps. One also can have the reaction increase the number of moles of material. The resulting expansion in volume would be another driver for the shock wave [2]. Yet another effect of this would be to introduce an entropic penalty to back-reaction and make the model more closely approximate the ZND assumption of irreversibility.

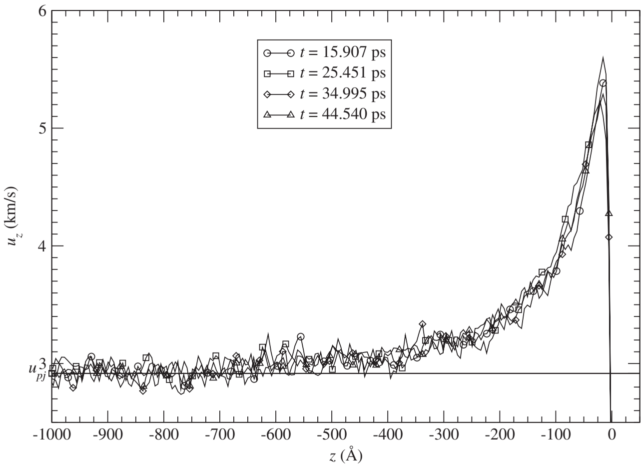

FIG. 7. Overlap of profiles of the z component of the particle velocity for a critically supported NEMD simulation using ModelIV parametrized such that $D_e^{AB}=1.0$ eV and $Q=4.0$ eV. A constant line is drawn at the CJ value of the particle velocity (u_{pj}), at which the driving piston is moving. Using a critically supported NEMD as opposed to an unsupported one drastically reduces the transient time from initiation to steady state [3].

To find the critical piston velocity in the preceding analysis, the CJ state for ModelIV is found by conducting NVE simulations and seeking the values of E and v that satisfy the Hugoniot jump conditions [3,14,21]. For ModelI $v_j/v_0 \approx 0.57$ and $u_{sj} \approx 9.7$ km/s [3]. From the results (see Table II), one should notice that for ModelIV the CJ state is less compressed than for ModelI and that u_{sj} is faster. Compared to conventional explosives, which typically have specific volumes $v_j/v_0 \approx 0.75$ and shock velocities $u_{sj} \approx 6$ km/s (for example, PETN [11]), ModelIV detonation fronts are over twice as fast and its CJ state is slightly less compressed. Note, however, that it has been shown for these REBO potentials that 3D simulations have lower, and therefore more realistic, velocities than do 2D ones [4,22]. Heim *et al.* [3] show how closely the conditions of the final state in a detonation of a ModelI material match those of the CJ conditions.

TABLE II. Determined thermodynamic values at CJ for ModelIV, where v is the specific volume, u_s is the shock velocity, u_p is the particle velocity, T is the temperature, U is the potential energy, E is the internal energy, P is the pressure, and λ is the degree of reaction. Subscript j indicates the CJ value, subscript 0 indicates the value at the initial state. Averages are per particle. The parentheses indicate the standard error in the two least significant digits of the mean.

v_j/v_0	0.789851(39)
u_{sj} (km/s)	13.87868(50)
u_{pj} (km/s)	2.91658(44)
$\langle k_BT_j \rangle$ (eV)	0.9185(84)
$\langle U_j \rangle$ (eV)	−0.8631(72)
$\langle E_j \rangle$ (eV)	0.0554(12)
P_j(eV/Å^2)	0.83846(16)
λ_j	0.8548516(36)

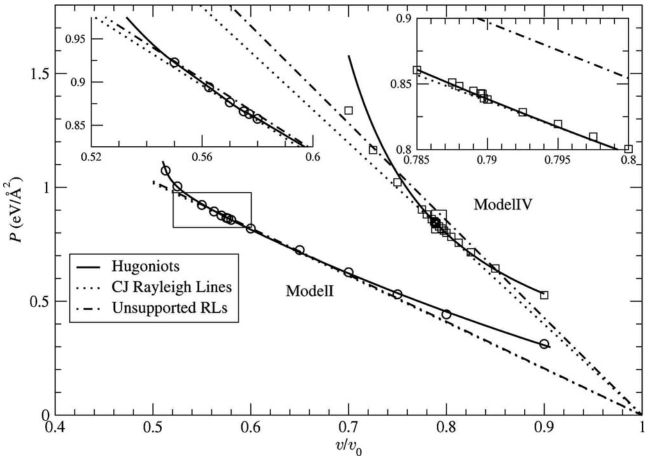

FIG. 8. Hugoniots for ModelI (circles) and ModelIV (squares). Solid lines are a guide to the eye for ModelI and a fit for ModelIV. Rayleigh lines are determined by the initial conditions and slopes. Dotted lines represent Rayleigh lines, the slopes of which are determined by the respective CJ values of the detonation velocity. Slopes of dash-dotted lines are determined by the average velocity of the shock waves in unsupported detonations. Boxes are magnifications.

For contrast, in Fig. 8 one can see that the Rayleigh line for the unsupported simulation is significantly steeper than for that of the CJ state.

In ZND theory this would require that the final state for ModelIV is either at a strong point or a weak point. The strong point is unstable and will only be a solution to the conservation equations if the detonation is overdriven. In the strict ZND theory there is no path to the weak point. ZND is, however, based on assumptions not realized by ModelIV. ModelIV has a reversible reaction, the pathway of which includes an endothermic dissociation. Endothermic steps can be responsible for weak point final states [2]. Perhaps the repulsive core introduced in ModelIV, by sheltering the dimers, prevents the reduction of the activation energy of the dissociative step and, hence, increases that step's reaction time, thus making it a stronger contributer to the overall reaction rate and causing the final state to be at a weak point. As is shown in the following paper [13] and can be inferred from Fig. 6, however, a 1D theory is not totally appropriate for this model.

In order to confirm that the modifications to the REBO model in the ModelIV potential do, indeed, maintain a dimerized state, the radial distribution function (RDF) at the CJ state is plotted. In Fig. 9 the CJ state of ModelIV is compared to that of ModelI. From the RDF for ModelIV, one can see that, after the peak at $r=r_e$, the curve drops to nearly zero while the analogous region in the RDF of ModelI is closer to unity. This is indicative of a molecular state for ModelIV and a dissociative state for ModelI. From Fig. 10 it is clear that the snapshot of the ModelIV CJ state supports the finding of the corresponding RDF. The snapshot for ModelI shows many more clusters and dissociated atoms.

For these images, a bond is defined for each potential. Two particles, i and j, are considered bonded if $E_{b,ij}+KE_{\|,ij} < E_c$ and $r_{ij} < r_c$, where $E_{b,ij}$ is as in Eq. (1) for ModelIV and Eq. (2) for ModelI except that the outer sum is over only i and j. $KE_{\|,ij} \equiv \frac{1}{2}\mu|(\vec{v}_i-\vec{v}_j)\cdot\vec{r}_{ij}/r_{ij}|^2$. μ is the reduced mass of i and j. For ModelIV $E_c=\epsilon c$ and $r_c=\gamma_2$ (see Table I). For ModelI E_c is the peak of the inner spline on the V_{vdW} term and r_c is the location of that peak (see Fig. 2). It can be shown that for ModelI there exists no minimum above and within these cutoff values for all values of $\bar{B}_{ij}$. To be considered part of a dimer, a particle must be bonded to only one other particle that is bonded to no other. If the particle types are the same, it is a product dimer; if different, a reactant dimer. To be part of a cluster, a particle must be bonded to either multiple particles or to one other that is bonded to multiple particles. To be dissociated, a particle must be bonded to no other.

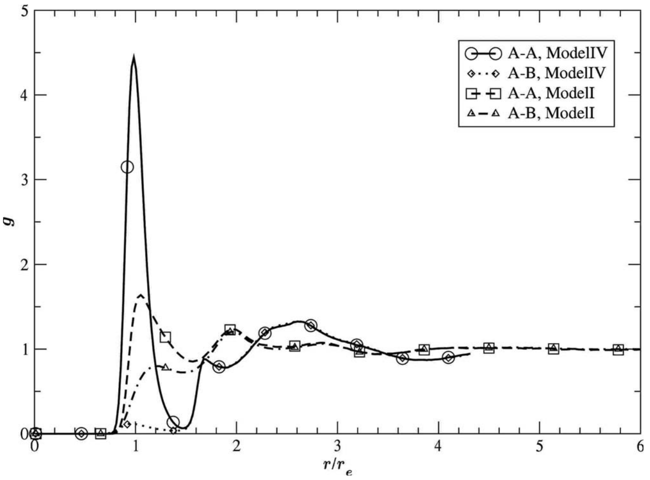

FIG. 9. Radial distribution functions for the CJ states of ModelIV and of ModelI.

With a bond defined, cookoffs that will reveal the reaction rate and the activation energy (E_a) for each model can be simulated. This is done for two reasons, to compare ModelIV to continuum models and to show another fortuitous difference between ModelI and ModelIV. The cookoffs are NVE

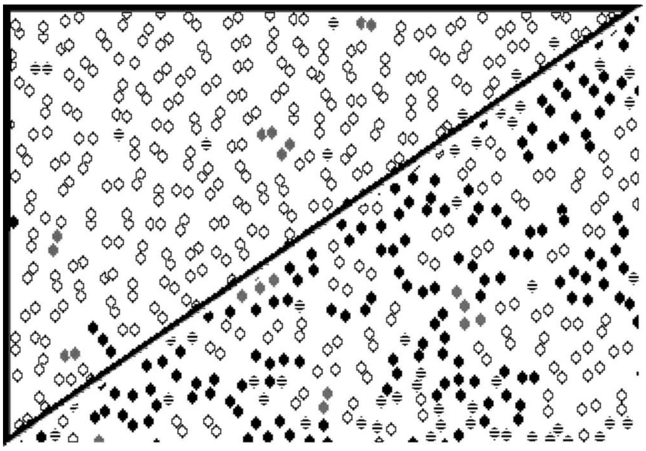

FIG. 10. Snapshots of the CJ state for ModelIV (upper) and ModelI (lower). Particles are marked by bond type. Gray atoms are in unreacted dimers; striped are unbonded, dissociated atoms; black are clustered atoms; and white are reacted dimers.

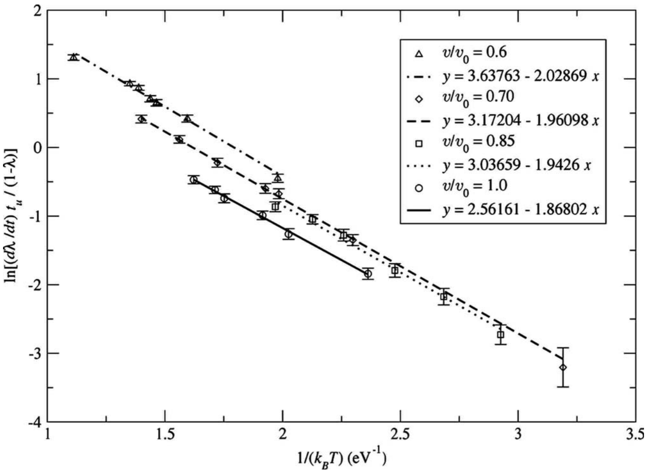

FIG. 11. Reaction rate of ModelIV for various internal energies and volumes vs temperature. Lines are fits to the Arrhenius form for constant volume. Their slopes are the negative of the activation energy. t_u is a unit of time and equals 10.180 505 fs.

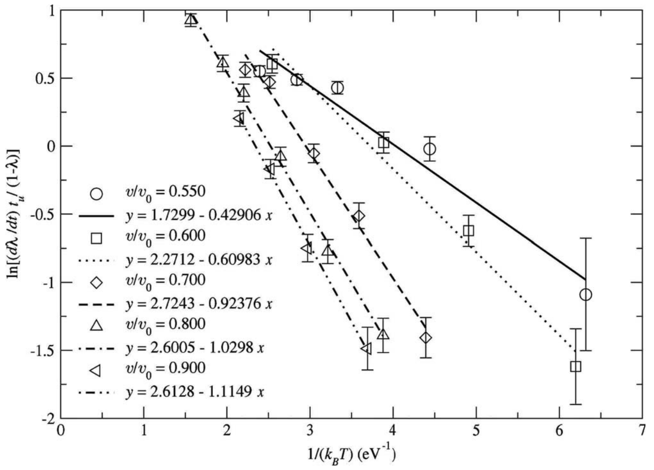

FIG. 12. Reaction rate of ModelI for various internal energies and volumes vs temperature. Lines are fits to the Arrhenius form for constant volume. Slope is the negative of the activation energy. t_u is a unit of time.

simulations started at different values of compression and internal energy but all with the initial *AB* chemical composition. As a simulation is started, thermal energy is partitioned among the different modes. After this has occurred and the reaction has progressed somewhat, the reaction rate is sampled over a short time and the temporal average of the rate and its standard error are recorded for the current simulation. In Fig. 11 the data are plotted for a series of simulations using the ModelIV potential. For each value of v, the data are fit to an Arrhenius reaction rate of the form [26]

$$\dot{\lambda} = (1-\lambda)A\exp\left[\frac{-E_a}{k_BT}\right], \tag{3}$$

where λ is the degree of reaction defined computationally as the ratio of reacted (defined as above) material to total amount of material. $\dot{\lambda}$ is the reaction rate and A is the frequency factor. The analogous plot for ModelI can be found in Fig. 12.

When contrasting the two figures, one notices that, over a similar range of volumes, ModelIV maintains a better fit to the Arrhenius form than ModelI and that the calculation of E_a remains relatively constant when compared to the E_a of ModelI. A probable contribution to the former observation is the manner in which a reaction is defined. At compressions typical in detonations, ModelI has a larger number of atoms in clusters and free states, which are not counted as reacted; only stable dimers are. One may consider a cluster of two *A* atoms tightly bonded together with a third, *B*-type particle loosely bonded to one of them as a state more reacted than one in which *A* is tightly bonded to *B* and loosely bonded to the other *A*. However, by our definition of reaction, all particles in a cluster are considered unreacted and only contribute to the denominator of the calculation of λ.

E_a for ModelI decreases with decreasing v. This is because at higher compressions an atom can have more neighbors within the bonding distance than with ModelIV. The bond-order coefficient then lowers the attraction between it and its neighbors, making it easier to break apart any existing bonds. For ModelIV, the repulsive core keeps neighbors away from dimers so that the bond-order coefficient and, thus, the dissociation energy remain unaffected by the same level of compression that would otherwise cause ModelI's dissociation energy to be reduced. For ModelIV there is a higher tendency than for ModelI for the compression to use up the space between dimers than that between the dimers' constituents. This is because for the former case a third particle would have to climb the repulsive core that was added to the V_{vdW} term before it got within the range of the cutoff function f_c, where it can diminish the bond-order coefficient $\bar{B}_{ij}$. In the latter case a third particle would only need to overcome the barrier of ModelI's inner spline (see Fig. 2), which is small compared to the temperature for most situations considered in reaction and detonation. For ModelIV the activation energy goes up slightly with decreasing volume. The exact reason for this is not known at present, but simulations with ReaxFF on the high explosive RDX also show this trend [23]. This may be due to a slight dependence of the rate on pressure ignored in Eq. (3). E_a for ModelIV is roughly 1 eV greater than for ModelI. This is commensurate with the height of the repulsive core.

V. CONCLUSION

In this paper it is shown that the changes to the ModelI version of the REBO potential have reduced the amount of clustered and dissociated atoms at the CJ state (by RDF) if not throughout the reaction zone (by a snapshot of an NEMD simulation). The CJ state of ModelIV is at a less compressed state and ModelIV's reaction zone is wider than ModelI's. ModelI's unsupported detonation velocity is much better predicted by CJ theory, where ModelIV's propagates significantly faster. In the following paper [13] we investigate ModelIV's relative disparity more closely. The cookoff simulations reveal that ModelIV fits an Arrhenius reaction rate through a wider domain of compressions than does ModelI and it has a higher and less density-dependent activation energy.

It was put forth that this higher E_a causes the final state to be at a weak point since it might make more significant in the reaction rate the endothermic step of dissociation. Given, however, the 2D shape of the front in Fig. 6, such a 1D explanation is probably insufficient. Higher E_a's should increase the likelihood of 1D and 2D instabilities in detonation waves [24,25]. The current value of ≈ 2 eV is consistent with the presumed activation energies for many conventional HEs.

The goal of the current research is the improvement of REBO, which we believe we have achieved, mainly, by introducing increased atomic repulsion, which reduces the reaction cross section. It was shown that ModelIV's reaction zone is wider than with ModelI and that the CJ state is a molecular one. REBO's insensitivity to initiation is increased, and a thicker induction zone is introduced. The reaction rate now behaves in a more Arrhenius manner, and the product EOS behaves more like a polytropic gas as indicated by the hyperbolic shape of its equilibrium $\mathcal{H}$. Some measurements, for example, the adiabatic γ—as is shown in the following paper [13]—and the amount of compression at CJ, are more commensurate with conventional explosives [10]. However, some are not too close, for example, the reaction temperature and shock velocity. 3D simulations are needed to investigate how the changes truly compare to real experiments.

ACKNOWLEDGMENTS

The authors would like to thank Sam Shaw, Alejandro Strachan, Brad Holian, Tommy Sewell, Yogesh Joglekar, and David Hall for useful conversations. This material was prepared by the University of California under Contract No. W-7405-ENG-36 and Los Alamos National Security under Contract No. DE-AC52-06NA25396 with the U.S. Department of Energy. The authors particularly wish to recognize funding provided through the ASC Physics and Engineering Modeling program.

---

[1] D. W. Brenner, D. H. Robertson, M. L. Elert, and C. T. White, Phys. Rev. Lett. **70**, 2174 (1993); **76**, 2202(E) (1996).
[2] W. Fickett and W. C. Davis, *Detonation* (University of California Press, Berkeley, 1979).
[3] A. J. Heim, N. Grønbech-Jensen, T. C. Germann, E. M. Kober, B. L. Holian, and P. S. Lomdahl, Phys. Rev. E **76**, 026318 (2007).
[4] C. T. White, D. R. Swanson, and D. H. Robertson, in *Chemical Dynamics in Extreme Environments*, edited by R. A. Dressler (World Scientific, Singapore, 2001), p. 547.
[5] D. Heflinger, I. Bar, T. Ben-Porat, G. Erez, and S. Rosenwaks, J. Appl. Phys. **73**, 2138 (1993).
[6] X. Tao, X. Kang, and Z. Jiaheng, Mater. Sci. Eng., B **38**, L1 (1996).
[7] N. R. Greiner, D. S. Phillips, J. D. Johnson, and F. Volk, Nature (London) **333**, 440 (1988).
[8] L. E. Fried and P. C. Souers, Propellants, Explos., Pyrotech. **21**, 215 (1996).
[9] W. M. Howard, L. E. Fried, and P. C. Souers, in *Eleventh Symposium (International) on Detonation*, Snowmass Village, CO (US Office of Naval Research, Arlington, VA, 1998).
[10] C. L. Mader, *Numerical Modeling of Detonations* (University of California Press, Berkeley, 1979).
[11] F. H. Ree, J. Chem. Phys. **81**, 1251 (1984).
[12] G. L. Schott, M. S. Shaw, and J. D. Johnson, J. Chem. Phys. **82**, 4264 (1985).
[13] A. J. Heim, N. Grøbech-Jensen, E. M. Kober, and T. C. Germann, following paper, Phys. Rev. E **78**, 046710 (2008).
[14] B. M. Rice, W. Mattson, J. Grosh, and S. F. Trevino, Phys. Rev. E **53**, 611 (1996).
[15] B. M. Rice, W. Mattson, J. Grosh, and S. F. Trevino, Phys. Rev. E **53**, 623 (1996).
[16] A. C. T. van Duin, A. Strachan, S. Stewman, Q. Zhang, X. Xu, and W. A. Goddard III, J. Phys. Chem. **107**, 3803 (2003).
[17] M. S. Shaw (private communication).
[18] J. F. Ziegler, J. P. Biersack, and U. Littmark, *The Stopping and Ranges of Ions in Solids, Vol. I* (Pergamon, New York, 1985).
[19] B. L. Holian and D. J. Evans, J. Chem. Phys. **78**, 5147 (1983).
[20] P. S. Lomdahl, P. Tamayo, N. Grønbech-Jensen, and D. M. Beazley, in *Proceedings of Supercomputing 93* (IEEE Computer Society Press, Los Alamitos, CA, 1993), p. 520.
[21] J. J. Erpenbeck, Phys. Rev. A **46**, 6406 (1992).
[22] J.-B. Maillet, B. Crouzet, C. Matignon, L. Mondelain, and L. Soulard, in *Shock Compression of Condensed Matter—2003* (AIP, New York, 2004), Vol. 706, pp. 385–388, http://link.aip.org/link/?APC/706/385/1
[23] A. Strachan, E. M. Kober, A. C. T. van Duin, J. J. Oxgaard, and W. A. Goddard, J. Chem. Phys. **122**, 54502 (2005).
[24] H. I. Lee and D. S. Stewart, J. Fluid Mech. **216**, 103 (1990).
[25] M. Short and D. S. Stewart, J. Fluid Mech. **368**, 229 (1998).
[26] $(\lambda_e - \lambda)$ makes a more accurate coefficient, where λ_e is the equilibrium value of λ and could be a source of further temperature and density dependence.